Cement and Concrete Composites 169 (2026) 106554

Contents lists available at ScienceDirect

Cement and Concrete Composites

journal homepage: www.elsevier.com/locate/cemconcomp

# Nano $CaCO_3$ seeding for improving properties of limestone calcined clay cement through in-situ carbonation

Zhonghao Niu [a], Xiangming Zhou [a,*], Pengkun Hou [b,a,**], Mingqing Liu [a], Shuang Liang [a], Yuzhou Sun [c], Yi Zhao [d], Junjie Wang [e]

[a] Department of Civil & Environmental Engineering, Brunel University of London, Uxbridge, Middlesex, UB8 3PH, United Kingdom
[b] Shandong Provincial Key Lab for the Preparation & Measurement of Building Materials, School of Materials Science & Engineering, University of Jinan, Jinan, 250022, China
[c] School of Civil & Transportation Engineering, Henan University of Urban Construction, Pingdingshan, 467036, China
[d] School of Intelligent Construction and Civil Engineering, Zhongyuan University of Technology, Zhengzhou, 450007, China
[e] Department of Civil Engineering, Tsinghua University, Beijing, 100084, China

ARTICLE INFO

*Keywords:*
Aqueous carbonation
$CO_2$ sequestration
In-situ carbonation
Limestone calcined clay cement
Nano $CaCO_3$

ABSTRACT

This study proposes an effective strategy to simultaneously enhance the mechanical performance and $CO_2$ sequestration capacity of limestone calcined clay cement ($LC^3$) incorporating low-grade calcined clay through aqueous carbonation. 25% of the cement fraction in $LC^3$ was subjected to aqueous carbonation for 10 to 40 min with a water-to-solid ratio of 2.0, leading to the in-situ precipitation of nano-sized $CaCO_3$. A maximum $CO_2$ uptake of 15.78% was achieved after 40 min of carbonation. After mixing with the remaining materials of the LC3 formulation, the synergistic dilution and nucleation effects of in-situ nano $CaCO_3$ promoted the hydration of silicate and aluminate phases, thereby refining the pore structure of $LC^3$. At 3 days, the fraction of fine capillary pores (10-50 nm) increased remarkably, reaching 54% and 60% after 30 and 40 min of carbonation, respectively, and this refinement was largely preserved at 28 days. Consequently, the 28-day compressive strength of $LC^3$ mortars increased by 34.93% and 32.07% at carbonation durations of 30 and 40 min, respectively, compared with the control group. However, substantial consumption of portlandite during pre-carbonation constrained the later development of carboaluminate phases, which highlights a trade-off between enhanced early hydration and limited availability of secondary hydration products. These findings offer new insights into the role of in-situ $CaCO_3$ precipitation in modifying hydration and pore structure, demonstrating that aqueous carbonation is an effective route to enhance $LC^3$ performance while facilitating $CO_2$ sequestration.

## 1. Introduction

The cement industry is one of the major contributors to global energy consumption and $CO_2$ emissions, accounting for approximately 6-8% of total anthropogenic $CO_2$ emissions worldwide [1,2]. With the urgent challenges of global climate change, the development of low-carbon and high-performance cementitious materials has become a research priority. Since most $CO_2$ emissions arise from clinker calcination, reducing clinker content is a widely recognised promising strategy to mitigate the environmental impact of cement production [3].

Limestone Calcined Clay Cement ($LC^3$) has attracted increasing attention in recent years due to its reduced clinker factor and favourable mechanical performance [4,5]. By partially replacing clinker with calcined clay and limestone, $LC^3$ reduces clinker consumption of approximately 40-50%, resulting in a reduction of $CO_2$ emissions by about 30-40% per ton of cement, compared with Portland cement [6]. Moreover, the pozzolanic reactivity of calcined clay, combined with the synergistic effect of limestone, promotes the formation of dense hydration products, such as hemicarboaluminate (Hc) and monocarboaluminate (Mc) [7–9], thereby enhancing the mechanical properties and durability of the cementitious matrix. Nevertheless, $LC^3$ suffers from relatively slow early-age hydration and insufficient strength

* Corresponding author
** Corresponding author. Shandong Provincial Key Lab for the Preparation & Measurement of Building Materials, School of Materials Science & Engineering, University of Jinan, Jinan, 250022, China
*E-mail addresses:* Xiangming.Zhou@brunel.ac.uk (X. Zhou), pkhou@163.com (P. Hou).

https://doi.org/10.1016/j.cemconcomp.2026.106554
Received 9 October 2025; Received in revised form 30 January 2026; Accepted 26 February 2026
Available online 27 February 2026

development, which restricts its broader application [10,11].

In recent years, various nanoparticles have been explored as hydration accelerators in cement-based materials. Among them, nano-$SiO_2$ not only provides abundant nucleation sites but also reacts pozzolanically with $Ca(OH)_2$ to generate additional C-S-H, thereby enhancing later-age strength and structural homogeneity [12–14]. Nano C-S-H seeds serve as precursors or templates for the epitaxial growth of C-S-H, thereby providing the most direct and efficient contribution to hydration kinetics [15,16]. In contrast, nano $CaCO_3$ promotes hydration through a combined physical-chemical mechanism, since it not only provides filler and nucleation effects but also interacts chemically with reactive aluminates. Moreover, the polymorphs of $CaCO_3$ (calcite, aragonite, and vaterite) influence the fluidity and compressive strength of cement-based materials due to their differences in solubility and reactivity [17–19].

In $LC^3$, calcium carbonate plays a crucial role as a major constituent, actively participating in hydration by interacting with alumina phases and stabilising carboaluminate hydrates. While reducing the particle size to the nanoscale can promote these effects by providing additional nucleation sites, the external incorporation of nano $CaCO_3$ is often limited by agglomeration and poor dispersion, which can limit its efficiency [20,21]. This highlights the necessity for a method that ensures both high intrinsic reactivity and optimal dispersion.

To address these dispersion challenges, in-situ aqueous carbonation is proposed. Compared to dry carbonation and semi-dry carbonation, aqueous carbonation exhibits significantly faster reaction kinetics [22], a more uniform carbonation product distribution [23] and relatively simpler process control [24]. Distinct from traditional gas-solid carbonation, the process is primarily controlled by the aqueous diffusion of carbonate species ($CO_3^{2-}$/ $HCO_3^-$), generated through the dissolution of $CO_2$ in the solution. Specifically, calcium-bearing phases (e.g., $Ca(OH)_2$ and C-S-H) release calcium ions, which then react in situ through a "dissolution-precipitation" process to form nanoscale $CaCO_3$ and alumina-silica gel, thereby densifying the microstructure [19,25,26]. Notably, the high-water demand of $LC^3$ is highly compatible with the liquid-rich environment required for aqueous carbonation, ensuring efficient transport. Within the favourable environment, the in-situ generated nanoscale $CaCO_3$ serves as nucleation sites to promote cement clinker hydration [27]. The carbonated cement slurry, consisting of residues and filtrate obtained after varying carbonation durations, was blended with the other materials of the $LC^3$ binder. Subsequently, the effects of carbonation duration on fresh properties, mechanical strength, and microstructural development (hydration and pore structure) were analysed. Specifically, the hydration process of $LC^3$ incorporating carbonated cement slurry was investigated using X-ray diffraction (XRD), thermogravimetric analysis (TG), low-field nuclear magnetic resonance (LF-NMR), and scanning electron microscopy (SEM).

## 2. Materials and methods

### 2.1. Materials

In this study, commercially available P·I 42.5, produced by Shandong Cement Group, was used as the main binder. Calcined clay, with a strength activity index of 84.23% in accordance with ASTM C311 [28], was sourced from Nanjing, China. Calcium carbonate and gypsum, both supplied by Merck, were used as supplementary materials for the preparation of $LC^3$. The properties of these materials meet the relevant requirements specified in ASTM C618 [29].

The chemical and mineralogical compositions of the raw materials were determined using X-ray fluorescence (XRF) and quantitative X-ray powder diffraction (XRD), as presented in Table 1. The particle size distribution of each raw material is presented in Fig. 1. Polycarboxylate ether (PCE) superplasticiser was employed to maintain the comparable flowability of mortars [30,31].

**Table 1**
Chemical and mineralogical compositions of raw materials (*wt.*%).

| Oxide | Cement | Calcined clay | Limestone | Gypsum |
|---|---|---|---|---|
| $SiO_2$ | 18.5 | 55.95 | 0.36 | 0.016 |
| $Al_2O_3$ | 3.99 | 34.62 | 0.25 | 0.017 |
| $Fe_2O_3$ | 3.40 | 1.79 | 0.06 | - |
| CaO | 59.17 | 0.91 | 54.07 | 49.48 |
| MgO | 3.79 | 1.75 | 0.40 | 0.02 |
| $SO_3$ | 3.41 | 0.14 | 0.09 | 50.44 |
| $Na_2O$ | 0.23 | 0.49 | - | 0.01 |
| $K_2O$ | 1.18 | 3.86 | 0.01 | 0.01 |
| $TiO_2$ | 0.25 | 0.28 | 0.01 | - |
| $M_nO$ | 0.09 | 0.02 | - | - |
| $P_2O_5$ | 0.08 | 0.05 | - | - |
| LOI | 1.87 | 1.07 | 43.04 | 20.91 |
| $C_3S$ | 63.66 | | | |
| $C_2S$ | 13.64 | | | |
| $C_3A$ | 6.86 | | | |
| $C_4AF$ | 8.93 | | | |
| Anhydrite | 2.13 | | | |

### 2.2. Methodology

In this study, the $LC^3$ formulation employed was composed of 50% ordinary Portland cement, 30% calcined clay, and 15% limestone by mass. Additionally, 5% gypsum ($CaSO_4{\cdot}2H_2O$) was added as a regulator to control the setting behaviour of the binder, following the procedure established by Avet and Scrivener [7]. The water-to-binder ratio (w/b) was maintained at a constant value of 0.5 for all mixtures. To investigate the effect of aqueous carbonation on the hydration and microstructural development of $LC^3$, 25% of the cement was subjected to carbonation by immersion in an aqueous solution saturated with $CO_2$, at a water-to-cement ratio of 2.0 (see Table 2).

#### 2.2.1. Aqueous carbonation of cement suspensions

The aqueous carbonation experiments were conducted at ambient temperature and pressure in a 500 mL beaker containing a cement suspension prepared by mixing 100 g of cement with 200 g of deionised water. Before carbonation, the suspension was homogenised by magnetic stirring at 500 rpm for 3 min and maintained at the same stirring rate throughout the procedure to ensure uniform dispersion. High-purity $CO_2$ gas (purity >99.9%) was bubbled into the suspension at a flow rate of 1 L/min through an air stone positioned 1 cm below the liquid surface. The carbonated cement suspensions were designated $CO_2$-10, $CO_2$-20, $CO_2$-30, and $CO_2$-40, corresponding to carbonation durations of 10, 20, 30, and 40 min, respectively, with the uncarbonated suspensions used as the control group ($CO_2$-0). A schematic of the aqueous carbonation setup established in this study is presented in Fig. 2.

After carbonation, the suspension was blended with the remaining raw materials to prepare $LC^3$ mortars and pastes. To investigate the phase assemblage and microstructural changes induced by aqueous carbonation, part of the carbonated cement paste was separated by vacuum filtration, rinsed three times with isopropanol to stop further hydration and carbonation, and then centrifuged at 3000 rpm for 3 min. The recovered solids were subsequently vacuum dried at 40 °C for 72h to ensure complete removal of residual moisture and solvent, according to established procedures [27,32]. The dried samples were then characterised by X-ray diffraction (XRD), thermogravimetric analysis (TGA), $N_2$ adsorption-desorption (BET), and scanning electron microscopy (SEM).

#### 2.2.2. Preparation of $LC^3$ mortar and paste

The carbonated cement suspension was blended with a polycarboxylate ether (PCE) superplasticiser and subsequently mixed with the remaining cementitious materials to ensure uniformity and

**Table 2**
Mix proportions of $LC^3$ with and without carbonated cement paste.

| Sample ID | A (%) | B (%) | $CO_2$ Duration (min) | Calcined Clay (%) | Limestone (%) | Gypsum (%) | w/b | PCE (%) |
|---|---|---|---|---|---|---|---|---|
| $LC^3$-0 | 25 | 25 | 0 | 30 | 15 | 5 | 0.5 | 0.32 |
| $LC^3$-10 | 25 | 25 | 10 | 30 | 15 | 5 | 0.5 | 0.51 |
| $LC^3$-20 | 25 | 25 | 20 | 30 | 15 | 5 | 0.5 | 0.94 |
| $LC^3$-30 | 25 | 25 | 30 | 30 | 15 | 5 | 0.5 | 1.44 |
| $LC^3$-40 | 25 | 25 | 40 | 30 | 15 | 5 | 0.5 | 1.86 |

*A represents the proportion of cement used for in-situ aqueous carbonation.
B represents the remaining proportion of cement in $LC^3$

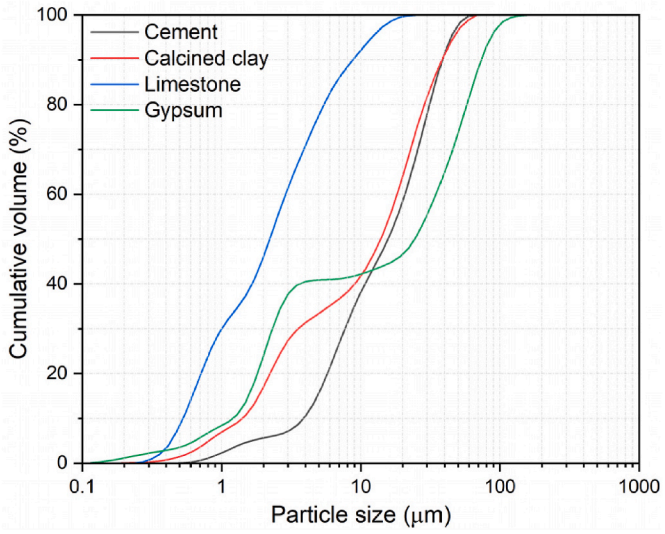


**Fig. 1.** Particle size distribution of raw materials.

consistency. Standard sand was added at a sand-to-binder mass ratio of 3:1, and the mixture was stirred for 5 min in a rotating mixer to produce mortar specimens. The fresh mortar was cast into 40 × 40 × 160 $mm^3$ prism moulds in accordance with EN 196-1, compacted by vibration, and covered with plastic film to minimise moisture loss. Curing was first carried out at 95% relative humidity and 20 ± 2 °C for 24h, after which the specimens were demolded and further cured under the same conditions until testing. The paste and mortar specimens were designated $LC^3$-0, $LC^3$-10, $LC^3$-20, $LC^3$-30, and $LC^3$-40, corresponding to carbonation durations of 0, 10, 20, 30, and 40 min, respectively, as summarised in Table 1.

### 2.3. Experimental methods

#### 2.3.1. Paste fluidity and setting time

After mixing the carbonated cement paste with the remaining constituents of the mixture for 3 min, the flowability of the $LC^3$ paste was tested using a flow table according to GB/T 2419-2005 [33]. A truncated cone mould (36 mm × 60 mm × 60 mm) was filled with the paste and lifted vertically, and the table was operated to complete 25 drops within 25 ± 1 s. The spread diameter was measured in two perpendicular directions, and their average was taken as the flow value. Each mixture was tested in triplicate, and the mean result was reported and quoted in the analyses.

The setting time of the $LC^3$ paste was measured using a Vicat apparatus in accordance with GB/T 1346-2011 [34]. Fresh paste was placed

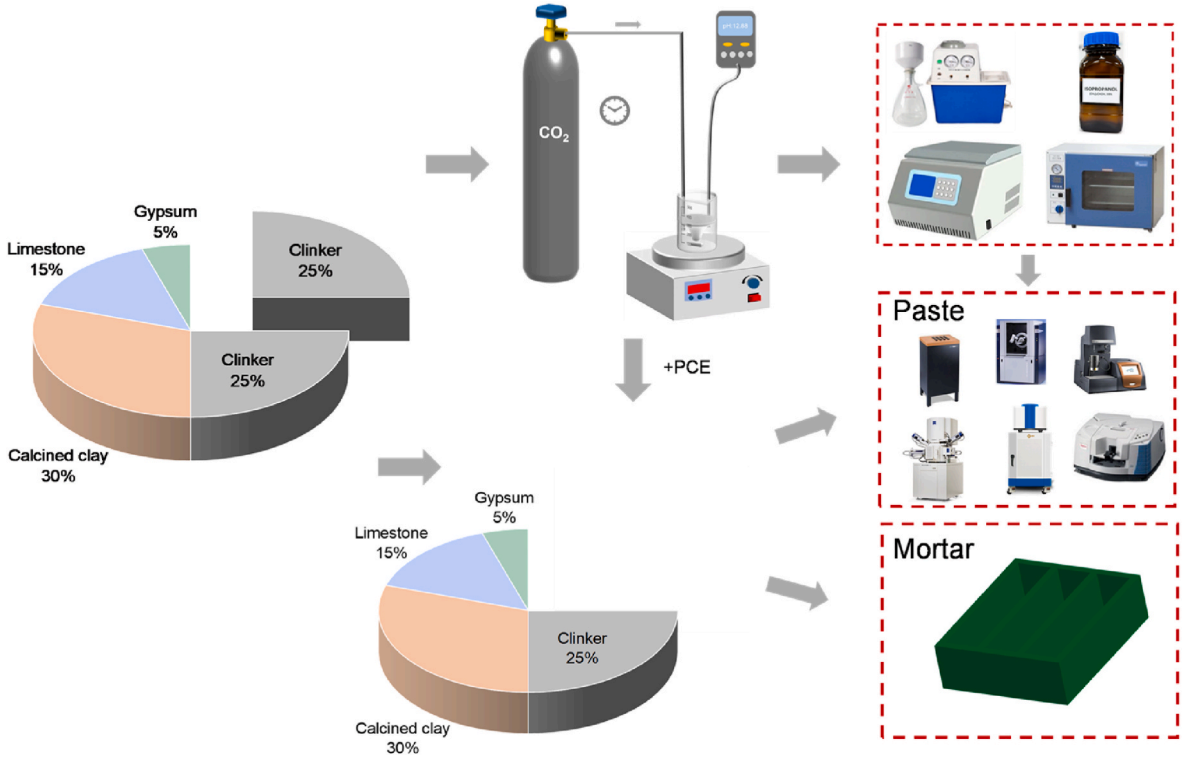


**Fig. 2.** Schematic view of in-situ carbonation preparation of $LC^3$.

into the Vicat mould and levelled, and the specimen was kept in a controlled environment at 20 ± 1 °C and relative humidity above 90%. The penetration of the Vicat needle was recorded every 5 min. Each mixture was tested in triplicate, and the mean value was reported and quoted in the analyses.

#### 2.3.2. Isothermal calorimetry

The $LC^3$ paste incorporating carbonated cement paste was homogenised via machine-assisted external mixing for 3 min. Subsequently, a sample of approximately 5.39 g was weighed out. The fresh paste was then immediately transferred into a sealed glass ampoule and placed in a TAM Air (8-channel, Thermometric, USA) isothermal calorimeter. Hydration heat flow and cumulative heat release were continuously recorded for 72h at 25 ± 0.1 °C to assess the early-age hydration kinetics influenced by the in-situ carbonated products. Two independent replicates were conducted to ensure reproducibility.

#### 2.3.3. Quantitative X-ray diffraction (QXRD)

Mineralogical identification and quantitative phase analysis of carbonated cement paste and hardened $LC^3$ paste were performed using a Bruker D8 Advance diffractometer (Cu-Kα radiation, λ = 1.54184 Å, 40 kV, 40 mA). For quantification, 0.8 g of ground paste (passing a 75 μm sieve) was homogenised with 0.2 g of α-$Al_2O_3$ as an internal standard (4:1 wt ratio) using ethanol as a dispersant. XRD patterns were recorded over a 2θ range of 5°-70° with a scanning speed of 2°/min and a step size of 0.02°. Phase quantification was performed via Rietveld refinement in TOPAS software. The refinement quality was confirmed by R*p* and R*wp* values below 15%, ensuring the reliability of the resulting phase contents.

The corresponding PDF code numbers used for phase identification are provided below: Alite (PDF# 00-042-0551), Belite (PDF# 00-029-0369), Ettringite (PDF# 00-041-1451), Gypsum (PDF# 00-021-0816), Portlandite (PDF# 00-004-0733), Calcite (PDF# 00-005-0586), Corundum (PDF# 00-010-0173), Hemi carboaluminate (PDF# 00-041-0221), Mono carboaluminate (PDF# 00-041-0219).

#### 2.3.4. Scanning electron microscopy (SEM)

The morphology of cement particles subjected to different carbonation durations was analysed using a ZEISS Gemini SEM 560 (Zeiss, Germany) equipped with energy-dispersive X-ray spectroscopy (EDS). Before imaging, the samples were rinsed with isopropanol to stop hydration, vacuum-dried at 40 °C for 72h, mounted on aluminium stubs, and sputter-coated with a thin gold layer to improve conductivity.

#### 2.3.5. Particle size distribution and specific surface area

The particle size distribution of raw materials and carbonated cement particles was measured using a Malvern Mastersizer 2000 (Malvern Instruments, UK). Specific surface area was determined by the BET method, while pore volume and size distribution were calculated using the BJH model from nitrogen adsorption-desorption isotherms (Kubo X1000). Differential pore volume curves from the adsorption branch were used to characterise pore structure.

#### 2.3.6. Thermogravimetric analysis (TGA)

The hydration of the paste samples was terminated using isopropanol, followed by drying in a vacuum oven at 40 °C for 3 days before TGA. The dried samples were subsequently ground to pass through a 75 μm sieve to ensure homogeneity. Thermogravimetric measurements were performed using a TGA 55 instrument. For each measurement, approximately 7 mg of the prepared powder was heated from 40 °C to 800 °C at a constant heating rate of 10 °C/min. To maintain an inert environment and prevent carbonation, a nitrogen flow of 50 mL/min was continuously applied throughout the heating process.

#### 2.3.7. Compressive strength of $LC^3$ mortar

The compressive strength of $LC^3$ mortar was measured from 40 mm-side length cubic specimens broken from 40 × 40 × 160 $mm^3$ prismatic samples by flexural bending after curing for 1, 3, 7 and 28 days under a loading rate of 2400 ± 200 N/s, and the average strength obtained from six cubic specimens from the same $LC^3$ formulation was recorded as the corresponding representative strength of the $LC^3$ at each curing age.

#### 2.3.8. Low field nuclear magnetic resonance (LF-NMR)

Low field nuclear magnetic resonance (LF-NMR) was employed to analyse the pore structure of $LC^3$ paste at 3d, 7d and 28d. For this purpose, a MicroMR20-025V NMR analyser (Niumag, China) operating at 20 MHz was employed to obtain the transverse relaxation time ($T_2$) distributions. Cylindrical specimens (Φ20mm × 20 mm) were fully saturated for 24h before testing to ensure complete pore filling. All measurements were conducted at 25 ± 1 °C, and the average value of three specimens of the same $LC^3$ formulation was taken as the corresponding representative value of the mixture for analysis.

## 3. Results and discussion

### 3.1. Characterisation of carbonated cement paste

#### 3.1.1. Particle size distribution and specific surface area

During aqueous carbonation, $CO_2$ dissolves into the solution to form carbonic acid, which subsequently dissociates into bicarbonate and carbonate ions under the high-alkaline environments. Meanwhile, the progressive dissolution of clinker phases, particularly $C_3S$, $C_2S$, and portlandite, reduces the particle size of cement grains and substantially increases their specific surface area (SSA) (Fig. 3), thereby enhancing ion exchange and reactivity. The released $Ca^{2+}$ interacts with carbonate species to precipitate $CaCO_3$, primarily as amorphous or nano-sized crystallites nucleating on cement particle surfaces. As the carbonation duration increases from 0 to 40 min, the particle size distribution of the carbonated cement powders progressively develops a bimodal pattern, indicating the coexistence of very fine particles and larger agglomerates, which suggests partial flocculation and heterogeneous carbonation of the cement grains. This coupled dissolution-precipitation process also refines the particle morphology (Fig. 4(b)) and increases the density of nucleation sites. SEM-EDS analysis confirms the formation of nanoscale $CaCO_3$, and it can be observed that nanoscale $CaCO_3$ and gel phases are interspersed on the surface of carbonated cement particles.

#### 3.1.2. Mineralogical phase

As shown in Fig. 5, the XRD patterns reveal that calcite peaks became

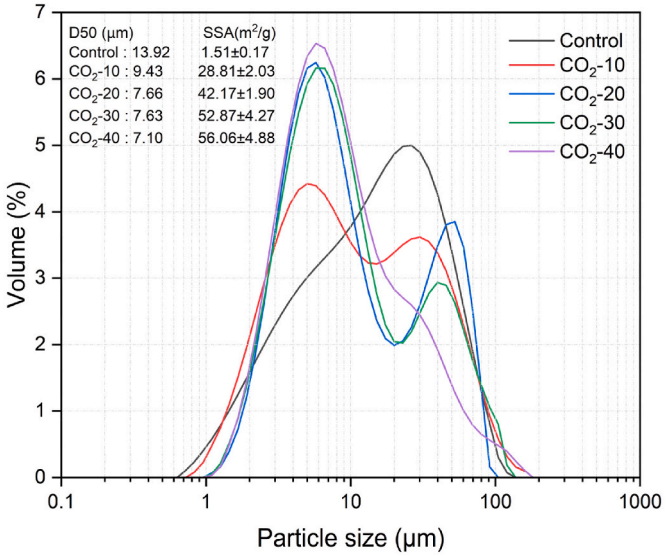


**Fig. 3.** Particle size distribution of carbonated cement particles.

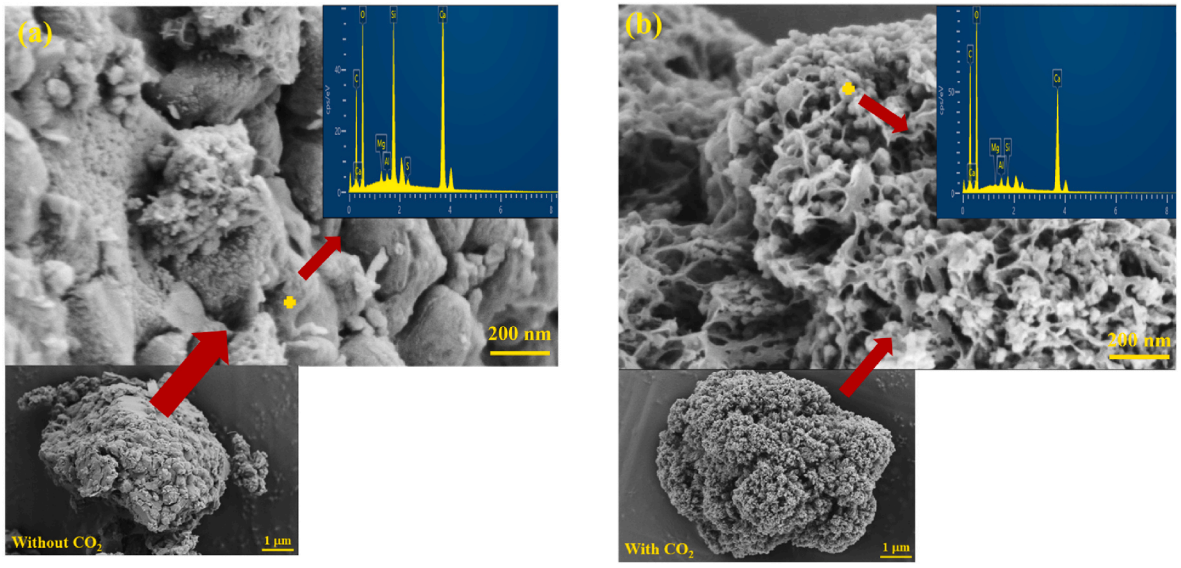


**Fig. 4.** Cement particles (a) without $CO_2$ and (b) with $CO_2$, 30 min.

more distinct with prolonged carbonation and the pH monitoring indicated that all carbonated specimens maintained a high alkalinity, with values remaining above 11.20 throughout the testing period. This high alkalinity, combined with the formation of calcite, indicates the ongoing hydration and carbonation of the calcium silicates ($C_3S$ and $C_2S$). Meanwhile, the progressive reduction and disappearance of the gypsum peak at 11.62° were observed, suggesting their decomposition and transformation during carbonation.

The quantitative changes in major phases were analysed by Rietveld refinement. As shown in Fig. 6, the contents of the amorphous phase and calcite varied markedly with carbonation duration, while the $CaCO_3$ content remained nearly constant after 30 and 40 min of carbonation. The crystallite size was evaluated by Rietveld refinement based on the Fundamental Parameter Approach via TOPAS [35], ranging from 36 to 75 nm. This nanoscale morphology is consistent with the SEM-EDS observations shown in Fig. 4, which reveal the formation of nanoscale $CaCO_3$ particles. The formation of these nanoscale $CaCO_3$ is associated with an increase in specific surface area, thereby providing nucleation sites for continued hydration, as reported by Monkman et al. [20,36].

The formation and content variation of $CaCO_3$ were further supported by the subsequent DTG analysis, which quantified the $CO_2$ uptake and phase evolution during the aqueous carbonation. As shown in Fig. 7

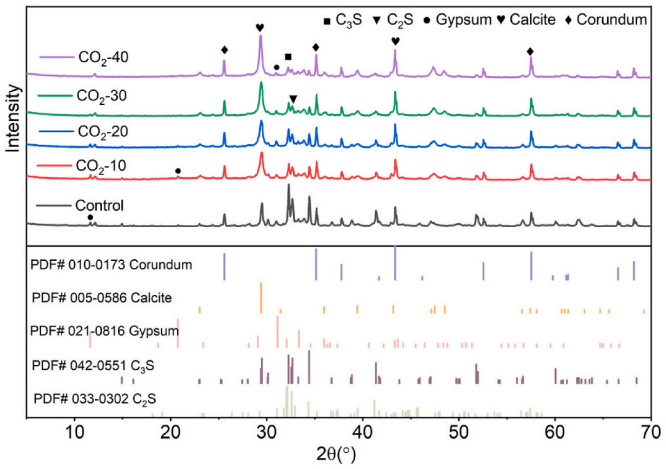


**Fig. 5.** XRD patterns of carbonated cement particles at different carbonation durations.

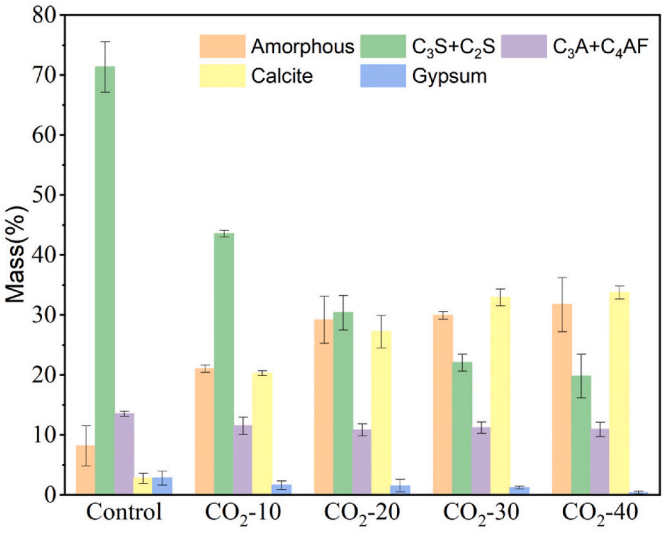


**Fig. 6.** Mineralogical evolution via QXRD.

(b), the broad peak in the 40-80 °C range and the sharp peak at approximately 105 °C are attributed to the dehydration of minor amounts of gel phases (including C-(A)-S-H and silica gel) and gypsum, respectively. With the progression of carbonation, C-(A)-S-H was readily decalcified to form $CaCO_3$ and silica gel, resulting in an increased intensity of the broad peak at 40-80 °C, while the gypsum peak diminished. Concurrently, the broad peak between 400 and 580 °C, associated with amorphous $CaCO_3$ [37], was observed. Furthermore, the sharp peak in the range of 580-700 °C, corresponding to the decomposition of calcite [38], exhibited a significant increase in intensity. The progressive increase in peak intensity with extended carbonation duration reflects the accumulation of stable carbonate phases within the cement matrix. Fig. 8 compares the $CO_2$ uptake obtained by the QXRD and DTG analyses, calculated based on Equations (1) and (2), respectively, in which $m_{co_2}$ denotes the molar mass of $CO_2$, while $M_n$ denotes the mass percentage of the sample at $n$°C.

$$\text{QXRD}: CO_2 \text{ uptake (wt. \%)} = M_{CaCO_3} \times \frac{m_{CO_2}}{m_{CaCO_3}} \quad (1)$$

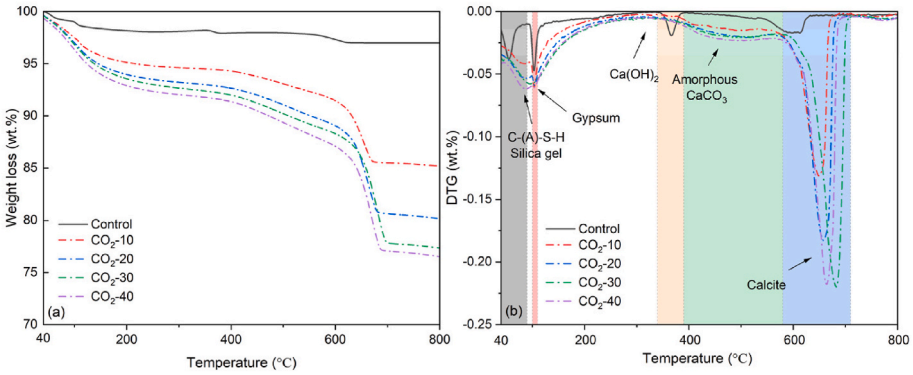


**Fig. 7.** (a) TG and (b) DTG results of carbonated cement particle.

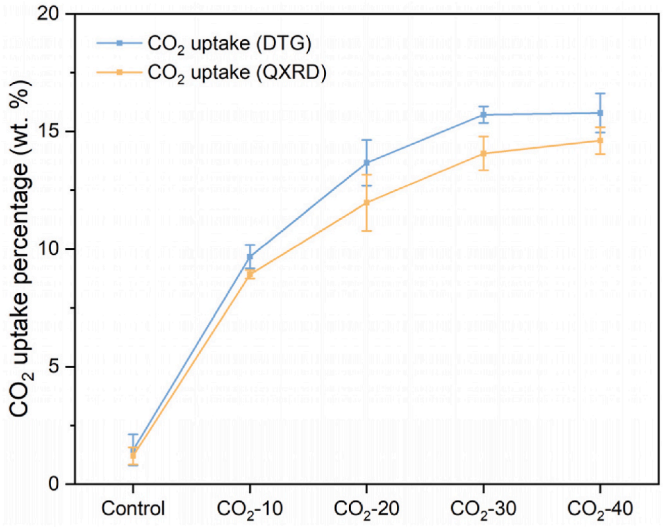


**Fig. 8.** Comparison of $CO_2$ uptake calculated by QXRD and DTG.

$$\text{DTG}: CO_2\ \text{uptake}\ (\text{wt. \%}) = \frac{M_{400} - M_{700}}{M_{105}} \times 100 \quad (2)$$

The results show that the $CO_2$ uptake determined by DTG is slightly higher due to the presence of amorphous $CaCO_3$. Nevertheless, both methods indicate that the $CO_2$ uptake was in the range of 15-16% after 30 min of carbonation.

### 3.2. Integration of in-situ carbonation with $LC^3$

#### 3.2.1. Fluidity and setting time of $LC^3$ paste

As shown in Fig. 9, the calcium carbonate generated during pre-carbonation markedly reduced both the fluidity and setting time of $LC^3$. Specifically, the initial and final setting times of $LC^3$-40 decreased by 44.60% and 41.67%, respectively, while the fluidity of $LC^3$-30 and $LC^3$-40 decreased by 34.25% and 36.64%. These changes can be primarily attributed to the participation of free water in hydration and carbonation reactions during pre-carbonation, which promotes the in-situ formation of nano-$CaCO_3$ and silica gel. The presence of these in-situ nucleated nano-$CaCO_3$ significantly accelerates subsequent cement hydration by providing abundant nucleation sites, thereby shortening the setting time and reducing workability [39]. Moreover, although carbonation decreases the amount of reactive clinker, the metakaolin fraction remains unchanged and retains its high specific surface area. Consequently, its strong water demand and pronounced thickening effect become more dominant, further contributing to the reduction in fluidity and the acceleration of setting [40].

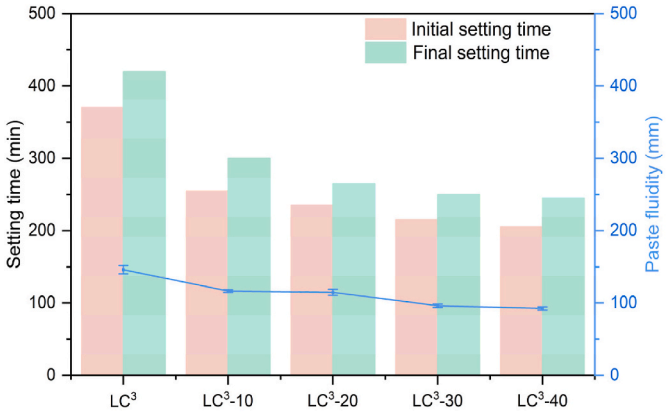


**Fig. 9.** Setting time and fluidity of $LC^3$ paste with carbonated cement paste.

#### 3.2.2. Compressive strength

The compressive strength results demonstrate that the in-situ formation of $CaCO_3$ significantly enhanced the compressive strength of $LC^3$ mortar over the curing period. For $LC^3$-10, short-duration carbonation had a negligible influence, showing values only comparable to the control group (Fig. 10). With longer carbonation duration, $LC^3$-20, $LC^3$-30, and $LC^3$-40 exhibited significantly higher strength. At 28d, the compressive strength of $LC^3$-10, $LC^3$-20, $LC^3$-30, and $LC^3$-40 increased

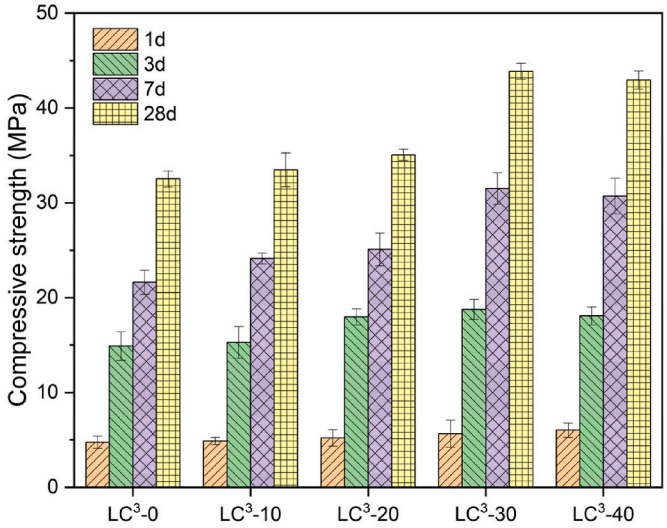


**Fig. 10.** Compressive strength of $LC^3$ subject to different carbonation durations.

by 2.98%, 7.81%, 34.93%, and 32.07%, respectively, compared to that of the control group, as shown in Fig. 11. Despite the relatively low reactivity of the calcined clay used in this study (Reactivity index of only 84.23%), $LC^3$-30 and $LC^3$-40 achieved compressive strengths of 43.88 and 42.95 MPa, respectively, at 28d, comparable to the EN 197-1 strength class CEM I 42.5 (28d standard mortar strength $\geq$42.5 MPa).

Although part of the clinker was consumed during aqueous carbonation to form $CaCO_3$ and amorphous phases, the carbonated $LC^3$ mortar still exhibited higher compressive strength than the control group, underscoring the positive role of carbonate products in hydration. However, further prolongation of the carbonation duration did not lead to continuous strength development. The slightly lower early-age strength observed in $LC^3$-40 relative to $LC^3$-30 may be attributed to excessive carbonation, which consumed reactive clinker phases and produced a dense carbonate layer, thereby hindering subsequent hydration [41]. In contrast, significant strength gains were observed at later ages. This pronounced late-age strength gain is ascribed to the filler and nucleation effect of $CaCO_3$. Furthermore, the pozzolanic reactivity of silica-rich gel may have also contributed to this enhancement, as reported by Zajac et al. [42]. These points highlight the positive contribution of aqueous carbonation to the strength development of $LC^3$.

### 3.2.3. Isothermal calorimetry

Fig. 12 illustrates the heat flow and cumulative hydration heat curves of $LC^3$ pastes with and without carbonated cement paste over 72 h. As shown in Fig. 12(a), the silicate hydration peak (Peak I) for $LC^3$-40 appeared approximately 3.5 h earlier than that of $LC^3$-0, signifying accelerated hydration kinetics. Regarding aluminate hydration (Peak II), the impact of carbonation was even more pronounced. The onset of $LC^3$-40 advanced to 17.6 h, which is nearly 13 h earlier than that of $LC^3$-0, where the reaction only initiated after 24 h. Similarly, $LC^3$-30 also exhibited an onset before 24 h. These results confirm that $CaCO_3$ effectively promotes and accelerates the aluminate hydration process [7].

### 3.2.4. QXRD analysis of $LC^3$ paste

Fig. 13 quantifies the hydration product contents of the samples at 1d and 28d following duplicate sampling and Rietveld refinement. It reveals distinct differences in $CaCO_3$ and amorphous phase contents among the samples at 1d (Fig. 13(a)) and further indicates that extended carbonation results in a marked rise in calcite content with a concomitant reduction in clinker phase content. Notably, the amorphous phase

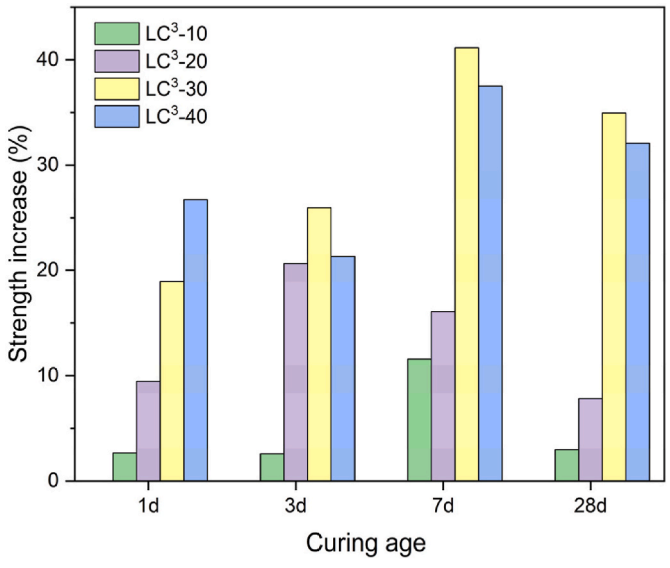


**Fig. 11.** Compressive strength increasing rates compared to $LC^3$-0 at various ages.

in $LC^3$-40 did not show a significant increase compared to that of $LC^3$-0. It appeared slightly lower than that of $LC^3$-20. However, the compressive strength results indicate that appropriate carbonation promotes early strength gain, suggesting that the early-age strength enhancement is not driven by the formation of additional C-S-H gel (amorphous phase) but primarily by the filler effect of the in-situ formed nanoscale $CaCO_3$, which densifies the microstructure.

Fig. 13(b) illustrates the quantitative phase assemblage of hydration products at 28d. In contrast to the results at 1d, the amorphous phase content increased significantly in all samples, becoming the dominant phase. Specifically, the amorphous content in carbonated samples ($LC^3$-10 to $LC^3$-40) ranged from 42% to 48%, surpassing that of the $LC^3$-0, which is around 39%. This substantial growth corresponds to the extensive formation of C-S-H gel and silica-rich gel derived from the pozzolanic reaction [37]. The 28d QXRD results reveal a marked reduction in Hc and Mc in $LC^3$-30 and $LC^3$-40, attributed to portlandite depletion, which constrains carboaluminate crystallisation [43]. Nevertheless, the long-term strength development was sustained by the high content of amorphous gel and residual calcite. The in-situ $CaCO_3$ served as effective nucleation sites, accelerating the precipitation of hydration products (C-(A)-S-H) and creating a dense matrix despite the limited presence of carboaluminate.

### 3.2.5. DTG analysis

Fig. 14 presents the DTG curves of samples at 1d and 28d, where four distinct peaks can be identified. The weight loss between 40 °C and 300 °C corresponds to the dehydration of C-(A)-S-H. The sharp peaks at around 80 °C and 120 °C correspond to the dehydration of AFt phase (ettringite) and AFm phases (Hc and Mc), respectively. The peak between 360 °C and 430 °C is associated with the dehydroxylation of calcium hydroxide, while the weight loss from 430 °C to 600 °C corresponds to the decomposition of amorphous calcium carbonate (ACC), which is less thermally stable than crystalline calcite. A strong peak at 600 °C - 700 °C is attributed to decarbonation of calcite.

Thermogravimetric analysis reveals a progressive increase in $CaCO_3$ content with longer carbonation durations, accompanied by enhanced compressive strength of early age, suggesting a positive correlation between carbonation products and mechanical performance. At 28d, a pronounced reduction in portlandite content was observed in all samples by DTG and QXRD. This reduction arises from early carbonation of clinker phases, the pozzolanic reaction of metakaolin, and the formation of Hc and Mc. These results further demonstrate that early-age precarbonation depletes part of the reactive $C_3S$ and $C_2S$, which consequently reduces the portlandite produced at later ages. In $LC^3$-30 and $LC^3$-40, excessive carbonation caused a pronounced deficiency of portlandite, thereby constraining AFm formation, whereas in the other groups, the peak intensity of AFm phases and C-(A)-S-H exhibited significant variation. As shown in Fig. 15, $LC^3$ with carbonated cement paste contained more $CaCO_3$ but less bound water (40 - 300 °C) compared to the control group. This suggests that the in-situ carbonation promotes a more uniform distribution of hydration products, which contributes positively to strength development.

### 3.2.6. Porosity analysis

To clarify the role of in-situ $CaCO_3$ in $LC^3$ hydration, pore structure analysis was performed using LF-NMR. Fig. 16 presents the total porosity of all samples at 3d and 28d as a function of carbonation duration. Short carbonation times, as in $LC^3$-10 and $LC^3$-20, resulted in higher porosity than the control group, whereas $LC^3$-30 displayed a porosity evolution comparable to the control group, suggesting that carbonation for 30 min exerts little influence on pore development. This behaviour can be explained by the evolution of PSD and SSA during carbonation: initially smooth cement grains progressively transformed into porous structures (Fig. 4). After 30 min, both D50 and SSA stabilised, confirming that carbonation duration governs the subsequent hydration and pore refinement of $LC^3$ paste. For $LC^3$-40, the porosity

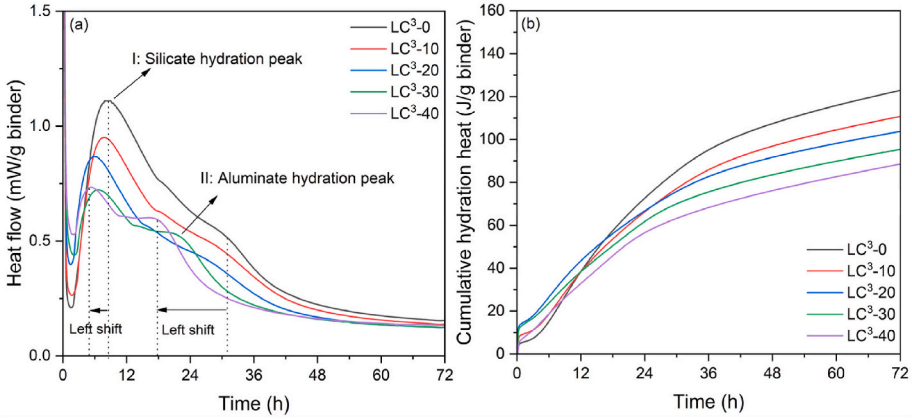


**Fig. 12.** (a) Hydration heat flow per unit binder mass. (b) Cumulative heat release per unit binder mass.

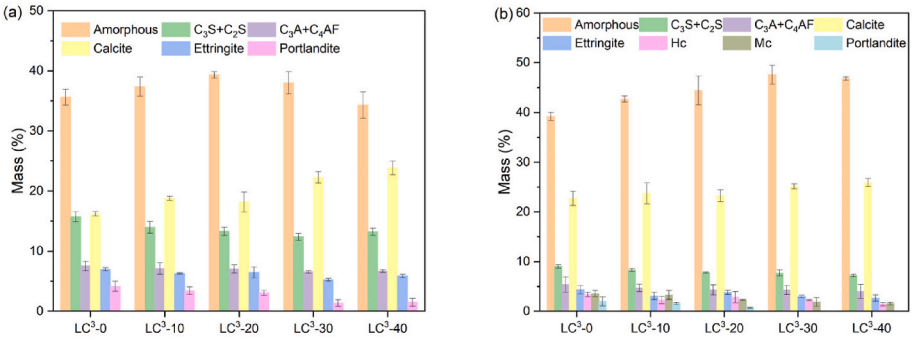


**Fig. 13.** QXRD results of $LC^3$ paste at (a) 1d and (b) 28d.

exhibits an initial increase followed by a subsequent decrease with hydration time, indicating that a carbonation duration of 40 min is already approaching an over-carbonation stage. From the SSA and fluidity results, it can be observed that after 30 min of carbonation, the SSA and fluidity of the cement particles gradually stabilise. At this stage, the silicate phases within the clinker undergo more pronounced dissolution and decalcification, together with significant alterations in their microstructural integrity, thereby reducing the amount of clinker that remains hydraulically active [44]. The progressively reduced compressive strength of $LC^3$-40 further supports these findings.

The LF-NMR results further reveal the pore size distribution of samples at 3d and 28d. Pore sizes were classified into four ranges: d < 10 nm (gel pores), 10-50 nm (fine capillary pores), 50 -100 nm (medium capillary pores), and d > 100 nm (coarse capillary pores) [45,46]. Macro-pores (50 nm-1 μm) are widely recognised as the dominant factors governing the strength and permeability of cementitious materials [47,48]. In this study, the pore volume distribution of all samples was mainly concentrated between 10 and 100 nm, indicating a predominantly mesoporous structure with limited macro-pore development, as shown in Fig. 17.

Fig. 17(a) shows the presence of distinct pore size peaks (d < 10 nm) in $LC^3$-0 and $LC^3$-10 at 3d, while the accompanying data in Fig. 17(b) quantifies the shifts in peak intensity and volume proportion. In contrast, samples subjected to longer carbonation durations displayed no pronounced peaks in this region, possibly due to the formation of nano $CaCO_3$, which promoted the densification of C-(A)-S-H. Compared with the control group, the primary pore volume distribution peaks of all samples, except $LC^3$-10, shifted toward smaller pore sizes and exhibited lower intensities, indicating refinement of gel pores and a reduction in overall gel pore volume. A small fraction of coarse capillary pores (>100 nm) was also detected in the carbonated samples. This may be attributed to the local dissolution of cement particles during aqueous carbonation and subsequent precipitation of nano $CaCO_3$, which can leave larger voids at original sites.

By 28d, the proportion of coarse capillary pores disappeared, as shown in Fig. 17(c). Meanwhile, the peak intensity of all samples incorporating carbonated cement paste was higher than that of the control, and the peak positions exhibited a progressive shift toward smaller pore sizes with increasing carbonation duration. A reduction in the proportion of pores >100 nm was identified, accompanied by an increase in fine capillary pores (10-50 nm), as shown in Fig. 17(d), the in-situ carbonation promoted the in-situ formation of calcium carbonate particles on the cement surface, which facilitated the further hydration of $LC^3$ cement clinker, thereby densifying its microstructure and improving its strength. The refinement effect was also particularly evident at 3d, with the fraction of fine capillary pores increased by 2.49%, 36.00%, 57.04%, and 71.95% for carbonation durations of 10, 20, 30, and 40 min, respectively. Although this refined distribution weakened over time, the proportion of fine capillary pores remained higher at 28d than that of the control. Such pore refinement, induced by $CaCO_3$ and amorphous phases, is expected to contribute positively to the strength development of $LC^3$, as shown in Fig. 18.

## 4. Conclusion

This study demonstrates that partial pre-carbonation of the $LC^3$ cement fraction produces in-situ nano sized $CaCO_3$ that reshapes early hydration, microstructure development, and mechanical performance through nucleation and dilution effects. First, in situ $CaCO_3$ supplies abundant nucleation sites that advance both the silicate (Peak I) and aluminate (Peak II) hydration events, increasing early cumulative heat on a binder basis. Afterwards, this nucleation advantage translates into rapid refinement within the mesopore band (10-50 nm), as evidenced by the leftward shift and intensification of PSD peaks and the elevation of

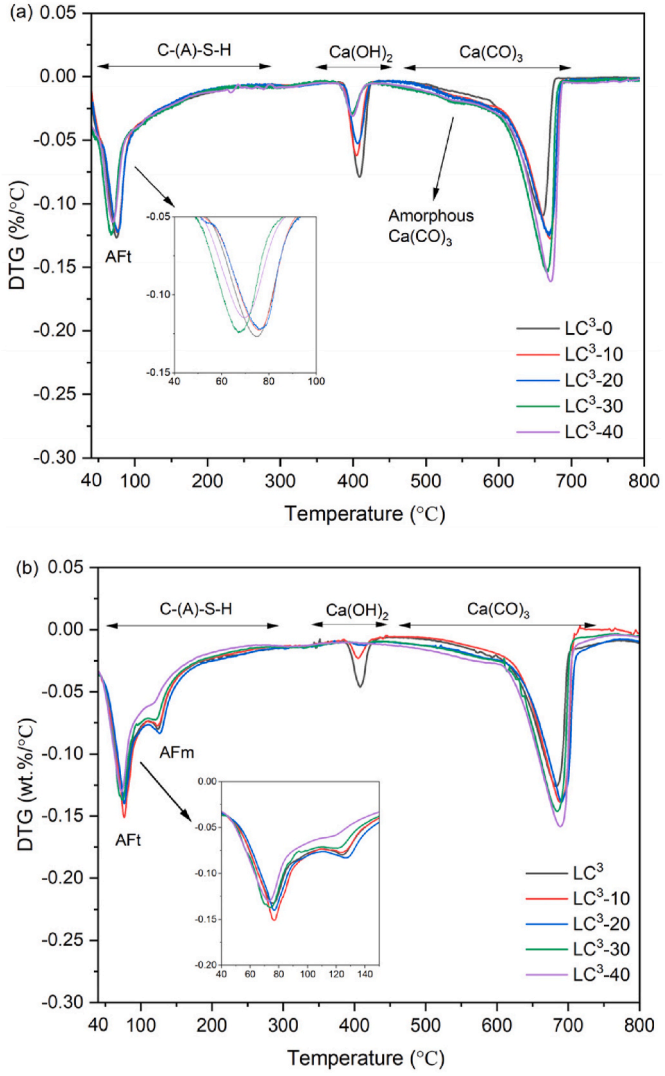


**Fig. 14.** DTG curve of $LC^3$ paste at (a)1 d and (b) 28 d.

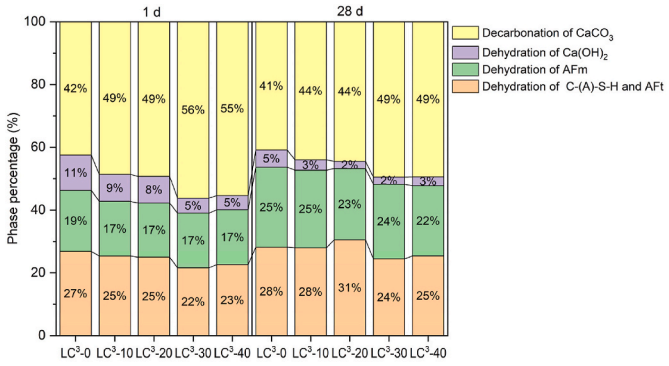


**Fig. 15.** Mass loss percentage of different hydration products in the samples.

the fine-capillary fraction to 28d. Moreover, the same pre-carbonation converts part of the reactive clinker into carbonate, progressively depleting portlandite and moderating the extent of carboaluminate (i.e. Hc and Mc) formation at later ages. Consequently, nucleation-driven densification surpasses clinker dilution within an optimal dosage, achieving pronounced strength gains. Considering both the process and property, 30 min of carbonation ($CO_2$ uptake ≈ 15%) was believed to be

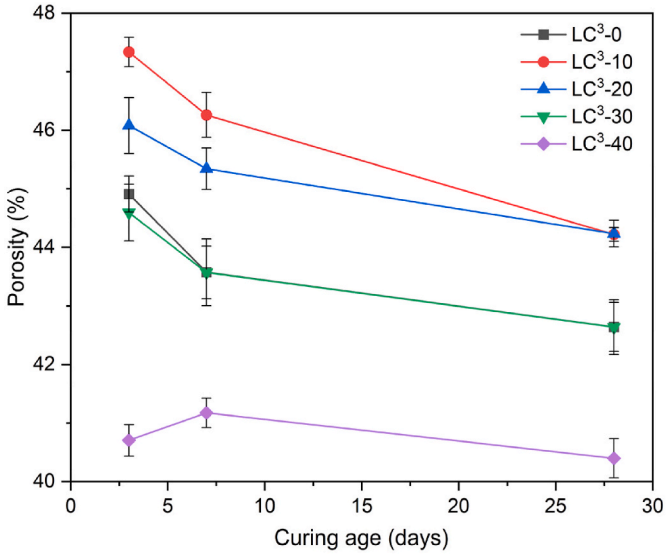


**Fig. 16.** Porosity evolution of $LC^3$ paste at different ages.

an optimum. $LC^3$-30 and $LC^3$-40 mortars exhibit about 30% higher 28d strength than the control group, approaching the EN 197-1 CEM I 42.5 strength class, despite the relatively modest reactivity of the calcined clay used. Nevertheless, at later ages, strength development is controlled by microstructural densification, indicating that the nucleation/filler roles of in situ $CaCO_3$ effectively compensate dilution up to a threshold. Based on the experimental results and analyses, the main conclusions can be drawn.

1) Aqueous carbonation led to the in-situ formation of nanoscale $CaCO_3$, which is interspersed with gel phase and adheres to the surface of cement particles. The increased specific surface area of the cement provided additional nucleation sites, effectively accelerating the hydration kinetics of silicate and aluminate phases in $LC^3$. However, the progressive consumption of portlandite during pre-carbonation restricted the later formation of hemicarboaluminate and monocarboaluminate, highlighting a trade-off between enhanced early hydration and limited availability of secondary hydration products.
2) In-situ generated nano $CaCO_3$ significantly improved the compressive strength of $LC^3$ mortar. At 28d, the strength of $LC^3$-30 and $LC^3$-40 increased by 34.93% and 32.7%, respectively, compared with the control, with 30 min identified as the optimum carbonation duration, corresponding to a $CO_2$ uptake of 15.71%.
3) The presence of in-situ formed nano-$CaCO_3$ refined the pore structure of $LC^3$, particularly within the 10-50 nm range. The proportion of fine capillary pores increased markedly at early ages and remained higher than the control at 28d, corresponding to long-term strength development.

From a sustainability perspective, the approach established in this study couples clinker reduction intrinsic to $LC^3$ with measurable $CO_2$ uptake during aqueous carbonation. The observed maximum uptake and the concurrent strength enhancement indicate a pathway to lower embodied $CO_2$ per unit performance. Practically, aqueous carbonation offers a controllable route to dispense nanoscale $CaCO_3$ without the dispersion challenge commonly associated with ex-situ nano-additions, mitigating agglomeration and improving spatial uniformity of nucleation sites. However, further investigation of long-term durability is needed, as the reduction in portlandite content resulting from in-situ carbonation limits AFm formation, which may influence durability that depends on $Ca(OH)_2$ and AFm (e.g., sulfate attack and chloride attack).

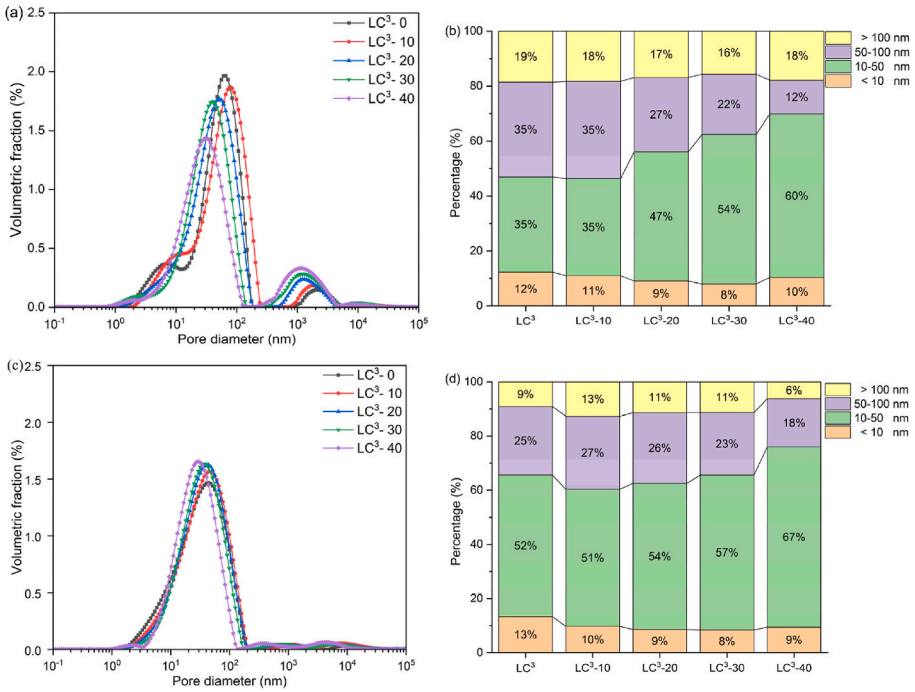


**Fig. 17.** Pore size distribution of samples at (a) (b) 3d and (c) (d) 28d.

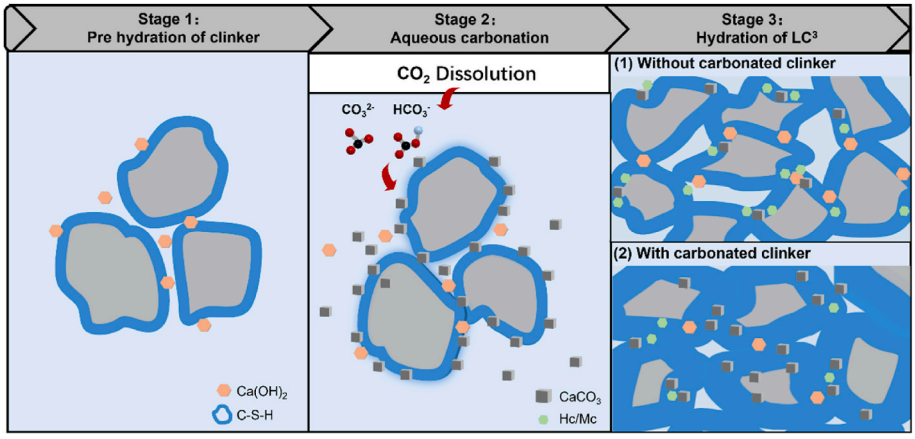


**Fig. 18.** Schematic diagrams of in-situ $CaCO_3$ formation and its impact on $LC^3$.

## CRediT authorship contribution statement

**Zhonghao Niu:** Writing – original draft, Methodology, Investigation, Formal analysis, Data curation, Conceptualization. **Xiangming Zhou:** Writing – review & editing, Supervision, Resources, Formal analysis. **Pengkun Hou:** Writing – review & editing, Supervision, Resources, Formal analysis, Conceptualization. **Mingqing Liu:** Writing – review & editing, Resources. **Shuang Liang:** Writing – review & editing, Resources. **Yuzhou Sun:** Writing – review & editing, Supervision, Resources. **Yi Zhao:** Writing – review & editing, Supervision, Resources. **Junjie Wang:** Writing – review & editing, Resources.

## Declaration of competing interest

The authors declare that they have no known competing financial interests or personal relationships that could have appeared to influence the work reported in this paper.

## Acknowledgement

The authors would like to thank the financial support from the UKRI under grant EP/X04145X/1 (i.e., the CSTO2NE project), the European Commission under grant 893469 (i.e. the NEASCMs project), the Royal Society under grant IEC\NSFC\223146, the Major Innovation Project of Guangxi Zhuang Autonomous Region (Grant No. 2024AA10004), and the China-Africa Joint Laboratory for Advanced Low-Carbon Cementitious Materials (Grant No. 2023YFE0126000). The first author would also like to thank Zhongyuan University of Technology for providing a partial PhD scholarship to him to proceed with this study at Brunel University of London.

## Data availability

Data will be made available on request.

## References


[1] F. Zunino, K. Scrivener, The reaction between metakaolin and limestone and its effect in porosity refinement and mechanical properties, Cement Concr. Res. 140 (2021) 106307, https://doi.org/10.1016/j.cemconres.2020.106307.

[2] T. Jiang, K. Cui, J. Chang, Development of low-carbon cement: carbonation of compounded C2S by β-C2S and γ-C2S, Cem. Concr. Compos. 139 (2023) 105071, https://doi.org/10.1016/j.cemconcomp.2023.105071.

[3] B. Lothenbach, K. Scrivener, R.D. Hooton, Supplementary cementitious materials, Cement Concr. Res. 41 (2011) 1244–1256, https://doi.org/10.1016/j.cemconres.2010.12.001.

[4] G.E. Abdelaziz, H. Shoukry, A.A. Selim, M.S. Saif, Recent progress in limestone-calcined clay cement (LC3): a review, in: Materials Science Forum, Trans Tech Publications Ltd, 2023, pp. 165–174, https://doi.org/10.4028/p-74p7so.

[5] K. Scrivener, F. Martirena, S. Bishnoi, S. Maity, Calcined clay limestone cements (LC3), Cement Concr. Res. 114 (2018) 49–56, https://doi.org/10.1016/j.cemconres.2017.08.017.

[6] K. Hosen, B. Chen, Limestone calcined clay cement (LC3): a review of materials, properties, production and environmental impact, J. Build. Eng. 112 (2025) 113672, https://doi.org/10.1016/j.jobe.2025.113672.

[7] F. Avet, K. Scrivener, Investigation of the calcined kaolinite content on the hydration of Limestone calcined clay cement (LC3), Cement Concr. Res. 107 (2018) 124–135, https://doi.org/10.1016/j.cemconres.2018.02.016.

[8] Y. Zhao, Y. Zheng, J. He, K. Cui, P. Shen, C.S. Poon, G. Peng, R. Guo, D. Xia, Development of reactive carbonate-calcined clay-cement (C4) composites through synchronizing aluminate-carbonate reaction: toward high compressive strength and low carbon emission, Cem. Concr. Compos. 160 (2025), https://doi.org/10.1016/j.cemconcomp.2025.106060.

[9] X. Qian, J. Wang, L. Wang, Y. Fang, Enhancing the performance of metakaolin blended cement mortar through in-situ production of nano to sub-micro calcium carbonate particles, Constr. Build. Mater. 196 (2019) 681–691, https://doi.org/10.1016/j.conbuildmat.2018.11.134.

[10] B. Liu, X. Gu, H. Wang, J. Liu, M.L. Nehdi, Y. Zhang, Study on the mechanism of early strength strengthening and hydration of LC3 raised by shell powder, J. Build. Eng. 98 (2024), https://doi.org/10.1016/j.jobe.2024.111422.

[11] Y. Yu, M. Yang, C. Wan, L. Lin, Mechanical, workability, economic and environmental properties of concrete with limestone calcined clay cement and recycled aggregates, Sci. Rep. 15 (2025), https://doi.org/10.1038/s41598-025-97539-6.

[12] M. Liu, X. Zhou, P. Hou, R. Hai, Y. Sun, S. Liang, Z. Niu, Effects of colloidal nanoSiO2 on the hydration and hardening properties of limestone calcined clay cement (LC3), Constr. Build. Mater. 411 (2024) 134371, https://doi.org/10.1016/j.conbuildmat.2023.134371.

[13] R.S. Lin, S. Oh, W. Du, X.Y. Wang, Strengthening the performance of limestone-calcined clay cement (LC3) using nano silica, Constr. Build. Mater. 340 (2022), https://doi.org/10.1016/j.conbuildmat.2022.127723.

[14] K. Khan, W. Ahmad, M.N. Amin, S. Nazar, Nano-Silica-modified concrete: a bibliographic analysis and comprehensive review of material properties, Nanomaterials 12 (2022) 1989, https://doi.org/10.3390/nano12121989.

[15] X. Li, J. Dengler, C. Hesse, Reducing clinker factor in limestone calcined clay-slag cement using C-S-H seeding – a way towards sustainable binder, Cement Concr. Res. 168 (2023) 107151, https://doi.org/10.1016/j.cemconres.2023.107151.

[16] E. Berodier, K. Scrivener, Understanding the filler effect on the nucleation and growth of C-S-H, J. Am. Ceram. Soc. 97 (2014) 3764–3773, https://doi.org/10.1111/jace.13177.

[17] D. Zhao, J.M. Williams, A.H.A. Park, S. Kawashima, Rheology of cement pastes with calcium carbonate polymorphs, Cement Concr. Res. 172 (2023) 107214, https://doi.org/10.1016/j.cemconres.2023.107214.

[18] D. Zhao, J.M. Williams, Z. Li, A.H.A. Park, A. Radlińska, P. Hou, S. Kawashima, Hydration of cement pastes with calcium carbonate polymorphs, Cement Concr. Res. 173 (2023) 107270, https://doi.org/10.1016/j.cemconres.2023.107270.

[19] Y. Zhou, F. Wu, L. Jinag, B. Lu, G. Hou, J. Zhu, Production of vaterite via wet carbonation of carbide residue: enhancing cement properties and CO2 sequestration, Cem. Concr. Compos. 150 (2024) 105549, https://doi.org/10.1016/j.cemconcomp.2024.105549.

[20] S. Monkman, Y. Sargam, L. Raki, Comparing the effects of in-situ nano-calcite development and ex-situ nano-calcite addition on cement hydration, Constr. Build. Mater. 321 (2022) 126369, https://doi.org/10.1016/j.conbuildmat.2022.126369.

[21] V.T. Nguyen, S.Y. Lee, D.J. Kim, Simulation of the effect of nano-CaCO3 agglomeration on the hydration process and microstructural evolution of cement paste, Case Stud. Constr. Mater. 19 (2023) e02612, https://doi.org/10.1016/j.cscm.2023.E02612.

[22] Y. Jiang, L. Peng, Z. Ma, J. xin Lu, P. Shen, C.S. Poon, Enhancing the treatment efficiency of recycled concrete fines with aqueous carbonation, Cement Concr. Res. 174 (2023), https://doi.org/10.1016/j.cemconres.2023.107338.

[23] Z. Liu, J. Du, W. Meng, Achieving low-carbon cementitious materials with high mechanical properties using CaCO3 suspension produced by CO2 sequestration, J. Clean. Prod. 373 (2022), https://doi.org/10.1016/j.jclepro.2022.133546.

[24] M. Zajac, J. Skibsted, P. Durdzinski, F. Bullerjahn, J. Skocek, M. Ben Haha, Kinetics of enforced carbonation of cement paste, Cement Concr. Res. 131 (2020) 106013, https://doi.org/10.1016/j.cemconres.2020.106013.

[25] M. Zajac, I. Maruyama, A. Iizuka, J. Skibsted, Enforced carbonation of cementitious materials, Cement Concr. Res. 174 (2023) 107285, https://doi.org/10.1016/j.cemconres.2023.107285.

[26] Z. Ma, Y. Jiang, J. He, P. Shen, Q. Qin, Z. Gu, J. Li, C.S. Poon, Revealing the connection between carbonation regimes and early pozzolanic reactivity of recycled concrete powder: impact of composition and microstructure, Cement Concr. Res. 186 (2024), https://doi.org/10.1016/j.cemconres.2024.107697.

[27] S. Luo, M. Wang, B.T. Pham, N. De Belie, T.C. Ling, Performance evaluation of mixing carbonated reactive magnesia slurry in Portland cement pastes, Cem. Concr. Compos. 160 (2025), https://doi.org/10.1016/j.cemconcomp.2025.106065.

[28] ASTM C311/C311M-18, Standard Test Methods for Sampling and Testing Fly Ash or Natural Pozzolans for Use in portland-cement Concrete, ASTM International, West Conshohocken, PA, 2018.

[29] ASTM C618, Standard Specification for Coal Fly Ash and Raw or Calcined Natural Pozzolan for Use in Concrete, 2015.

[30] L. Liu, Y. Ji, F. Gao, L. Zhang, Z. Zhang, X.Y. Liu, Study on high-efficiency CO2 absorption by fresh cement paste, Constr. Build. Mater. 270 (2021), https://doi.org/10.1016/j.conbuildmat.2020.121364.

[31] Z. Zhao, T. Qi, W. Zhou, D. Hui, C. Xiao, J. Qi, Z. Zheng, Z. Zhao, A review on the properties, reinforcing effects, and commercialization of nanomaterials for cement-based materials, Nanotechnol. Rev. 9 (2020) 349–368, https://doi.org/10.1515/ntrev-2020-0023.

[32] S. Monkman, Y. Sargam, O. Naboka, B. Lothenbach, Early age impacts of CO2 activation on the tricalcium silicate and cement systems, J. CO2 Util. 65 (2022) 102254, https://doi.org/10.1016/j.jcou.2022.102254.

[33] GBT 2419-2005, GB/T 2419, Method for Determination of Fluidity of Cement Mortar, Chinese Standards Association, China, 2005.

[34] GB/T 1346, Test Methods for Water Requirement of Normal Consistency, Setting Time and Soundness of the Portland Cement, Chinese Standards Association, China, 2011.

[35] S. Krishnan, S.K. Kanaujia, S. Mithia, S. Bishnoi, Hydration kinetics and mechanisms of carbonates from stone wastes in ternary blends with calcined clay, Constr. Build. Mater. 164 (2018) 265–274, https://doi.org/10.1016/J.CONBUILDMAT.2017.12.240.

[36] S. Monkman, B.E.J. Lee, K. Grandfield, M. MacDonald, L. Raki, The impacts of in-situ carbonate seeding on the early hydration of tricalcium silicate, Cement Concr. Res. 136 (2020) 106179, https://doi.org/10.1016/j.cemconres.2020.106179.

[37] M. Zajac, J. Skibsted, F. Bullerjahn, J. Skocek, Semi-dry carbonation of recycled concrete paste, J. CO2 Util. 63 (2022) 102111, https://doi.org/10.1016/j.jcou.2022.102111.

[38] Z. Yu, Y. Meng, K.H. Mo, H. Liu, T.C. Ling, Influences of w/c and CO2 curing duration on the high temperature properties of cement pastes, J. Build. Eng. 69 (2023) 106293, https://doi.org/10.1016/j.jobe.2023.106293.

[39] Q. Fu, Z. Zhang, X. Zhao, W. Xu, D. Niu, Effect of nano calcium carbonate on hydration characteristics and microstructure of cement-based materials: a review, J. Build. Eng. 50 (2022), https://doi.org/10.1016/j.jobe.2022.104220.

[40] F. Nazário Santos, S. Raquel Gomes de Sousa, A. José Faria Bombard, S. Lopes Vieira, Rheological study of cement paste with metakaolin and/or limestone filler using mixture design of experiments, Constr. Build. Mater. 143 (2017) 92–103, https://doi.org/10.1016/j.conbuildmat.2017.03.001.

[41] N. Saeki, L. Cheng, R. Kurihara, T. Ohkubo, A. Teramoto, Y. Suda, R. Kitagaki, I. Maruyama, Natural carbonation process in cement paste particles in different relative humidities, Cem. Concr. Compos. (2023) 105400, https://doi.org/10.1016/j.cemconcomp.2023.105400.

[42] J. Song, M. Zajac, M. Ben Haha, J. Skibsted, Impact of Ca/Si and Al/Si ratios on the composition and structure of the alumina-silica gel formed by wet carbonation of synthesized C-S-H in blends with portlandite and ettringite, Cement Concr. Res. 197 (2025), https://doi.org/10.1016/j.cemconres.2025.107931.

[43] F. Zunino, E. Zurich, J. Sun, K. Scrivener, Challenges and opportunities of LC3 with less than 50% clinker, n.d. https://www.researchgate.net/publication/374255810.

[44] Y. Jiang, L. Li, J. xin Lu, P. Shen, T.C. Ling, C.S. Poon, Mechanism of carbonating recycled concrete fines in aqueous environment: the particle size effect, Cem. Concr. Compos. 133 (2022), https://doi.org/10.1016/j.cemconcomp.2022.104655.

[45] B. Song, S. Liu, X. Hu, K. Ouyang, G. Li, C. Shi, Compressive strength, water and chloride transport properties of early CO2-cured Portland cement-fly ash-slag ternary mortars, Cem. Concr. Compos. 134 (2022) 104786, https://doi.org/10.1016/j.cemconcomp.2022.104786.

[46] Z. Yang, C. Zhou, Pore structure of water-saturated cement mortars by low-field nuclear magnetic resonance, J. Chin. Ceram. Soc. 50 (2022) 1391–1400, https://doi.org/10.14062/j.issn.0454-5648.20210660.

[47] X. Chen, S. Wu, J. Zhou, Experimental study and analytical model for pore structure of hydrated cement paste, Appl. Clay Sci. 101 (2014) 159–167, https://doi.org/10.1016/j.clay.2014.07.031.

[48] J. Zhu, R. Zhang, Y. Zhang, F. He, The fractal characteristics of pore size distribution in cement-based materials and its effect on gas permeability, Sci. Rep. 9 (2019), https://doi.org/10.1038/s41598-019-53828-5.